Electronic Supplementary Information (ESI)

Dual-templating synthesis of three-dimensionally ordered macroporous $La_{0.6}Sr_{0.4}MnO_3$-supported Ag nanoparticles: controllable alignments and super performance for the catalytic combustion of methane

Hamidreza Arandiyan,[a] Hongxing Dai,*[b] Jiguang Deng,[b] Yuan Wang,[b,c] Shaohua Xie[b] and Junhua Li*[a]

[a]*State Key Joint Laboratory of Environment Simulation and Pollution Control (SKLESPC), School of Environment, Tsinghua University, Beijing 100084, China*

[b]*Laboratory of Catalysis Chemistry and Nanoscience, Department of Chemistry and Chemical Engineering, College of Environmental and Energy Engineering, Beijing University of Technology, Beijing 100124, PR China*

[c]*National Research Center for Geoanalysis, Beijing 100037, China*

* Authors to whom correspondence should be addressed:

Prof. Hongxing Dai (H. X. Dai)

Tel. No.: +86-10-6739-6118; fax: +86-10-6739-1983

E-mail: hxdai@bjut.edu.cn

Prof. Junhua Li (J. Li)

Tel. No.: +86-10-6277-1093; fax: +86-10-6277-1093

E-mail: lijunhua@tsinghua.edu.cn

Content

Synthesis of the yAg/3DOM $La_{0.6}Sr_{0.4}MnO_3$ catalysts

The 3DOM $La_{0.4}Sr_{0.6}MnO_3$-supported silver (*y*Ag/3DOM $La_{0.4}Sr_{0.6}MnO_3$) catalysts were prepared via the dimethoxytetraethylene glycol (DMOTEG)-assisted gas-bubbling reduction methods. The typical preparation procedure is as follows: A desired amount of PEG400 (MW = 400 g/mol) and DMOTEG (MW = 222.28, D = 1.009 g/mL at 25 °C) was added to a 100 mg/L $HAgCl_4$ aqueous solution (Ag/DMOTEG mass ratio = 1.5 : 1) at RT under vigorous bubbling for 10 min. After rapid injection of an aqueous solution of 0.1 mol/L $NaBH_4$(Ag/$NaBH_4$ molar ratio = 1 : 5), one could obtain a dark brown solution (so-called silver sol). A desired amount (theoretical Ag loading = 2, 4 or 6 wt%) of the 3DOM $La_{0.4}Sr_{0.6}MnO_3$ support was then added to the silver sol, and the obtained suspension was subjected to sonication (60 kHz) for 30 s. A gas-bubble-assisted stirring operation with three bubble outlets in solution was used to further agitate the system, and the suspension was vigorously bubbled with N_2 for 8 h. The solid was collected by filtration, followed by washing with 2 L of deionized water. After obtaining a uniform precursor solution, ca. 3.00 g of highly ordered PMMA colloidal crystal microspheres was added and soaked with the above mixed solution. After the PMMA microspheres were thoroughly wetted, the excessive liquid was filtered via a Buchner funnel connected to vacuum (0.07 MPa). After being dried at room temperature (RT) for 24 h, the 3DOM materials were thermally treated in a tubular furnace according to the two steps: (a) heated in a N_2 flow of 50 mL/min at a ramp of 1 °C/min from RT to 300 °C and kept at this temperature for 3 h; and (b) after being cooled to 30 °C in the same atmosphere and purged in an air flow of 50 mL/min, the solid was heated at a ramp of 1 °C/min from RT to 300 °C and kept at this temperature for 1 h, and then at the same ramp from 300 to 800 °C and maintained at 800 °C for 4 h, as illustrated in

Scheme 1. The obtained samples were denoted as *y*Ag/3DOM $La_{0.6}Sr_{0.4}MnO_3$. For comparison purposes, we also prepared the Bulk $La_{0.6}Sr_{0.4}MnO_3$ sample. The Bulk $La_{0.6}Sr_{0.4}MnO_3$ sample was prepared using the citric acid-complexing method described elsewhere. The obtained solid precursor was first calcined in air at a ramp of 1 °C/min in a muffle furnace from RT to 300 °C and kept at this temperature for 1 h, and then from 300 to 800 °C the same ramp and maintained at 800 °C for 4 h. The results of inductively coupled plasma atomic emission spectroscopic (ICP-AES) investigation reveal that the real Ag loading was 1.58, 3.63, and 5.71 wt% for the *y*Ag/3DOM $La_{0.6}Sr_{0.4}MnO_3$ samples, respectively (Table 1). All of the above steps were carried out by covering all of the containers with a layer of aluminum foil. All of the chemicals (A.R. in purity) were purchased from Sinopharm Chemical Reagent Beijing Company and used without further purification.

Catalyst characterization procedures

The X-ray diffraction (XRD) experiments were performed on a Philips PW-1800 diffractometer using Cu Kα radiation (λ = 0.15406 nm) at 40 kV and 30 mA to determine the crystalline phases and to calculate lattice parameters. Scattering intensities were measured over an angular range of $4^{o} < 2\theta < 90^{o}$ for all of the samples with a step size (2θ) of 0.03^{o} and a count time of 2 s per step. The diffraction patterns were indexed by comparison with the JCPDS (Joint Committee on Powder Diffraction Standards) files. The morphologies of the as-prepared catalysts were studied by scanning electron microscopy (SEM) using a Philips XL30 microscope operating at an accelerating voltage of 30 kV, with a work distance (WD) between 10 and 13 mm. For the determination of the chemical compositions of the crystalline phases, energy-dispersive spectroscopy (EDS) was used to determine the EDS spectra using an EDS DX-4 analysis system. A very thin Au deposit was used to improve the conductivity of the sample. Transmission electron microscopic (TEM) images as well as the selected-area electron diffraction (SAED) patterns of the typical samples were recorded on a JEOL JEM-2010 apparatus. The N_2 adsorption-desorption isotherms, surface areas, and pore parameters of the samples were determined via N_2 adsorption at −196 ^{o}C on a Micromeritics ASAP 2020 adsorption analyzer. Before measurement, the samples were degassed at 250 ^{o}C for 3 h. The surface areas and pore size distributions were calculated using the Brunauer-Emmett-Teller (BET) and Barrett-Joyner-Halenda (BJH) methods.

Hydrogen temperature-programmed reduction (H_2-TPR) studies were performed with an Autochem II 2920 (Micromeritics) apparatus equipped with a TCD detector. The experiments were conducted on the samples (approximately 50 mg). The samples were initially flushed with helium at a flow rate of 40 mL/min as the temperature was increased at a ramp rate of 10 ^{o}C/min to 200 ^{o}C and held at this temperature for 30 min to remove water. Then, the reducing gas (5.1% H_2 in Ar) was introduced at a flow rate of 40 mL/min with a ramp rate of 10 ^{o}C/min from room temperature to 750 ^{o}C. The variation in H_2 concentration of the effluent was monitored on-line by the chemical adsorption analyzer. The reduction peak was calibrated against that of complete reduction of a known standard of powdered CuO (Aldrich, 99.995%).

X-ray photoelectron spectroscopic (XPS)

The X-ray photoelectron spectroscopic (XPS) technique was used to determine the La 3d, Sr 2p, Mn 2p, and O 1s binding energies (BEs) of surface lanthanum, strontium, manganese, and oxygen species with Mg Kα ($h\nu$ = 1253.6 eV) as the excitation source. Before XPS measurement, the sample was treated in an O_2 flow of 20 mL/min at 200 ^{o}C for 1 h. After being cooled to RT, the pretreated sample was transferred to a holder in a Glove Bag (Instruments for Research and Industry, USA) that was filled with helium, and then the holder was transferred into the spectrometer chamber under helium. The sample was outgassed (0.5 h) in the preparation chamber before being analyzed in the analysis chamber. The BE values of La 3d, Sr 2p, Mn 2p, and O 1s were calibrated against the C 1s signal (BE = 284.6 eV) of contaminant carbon.

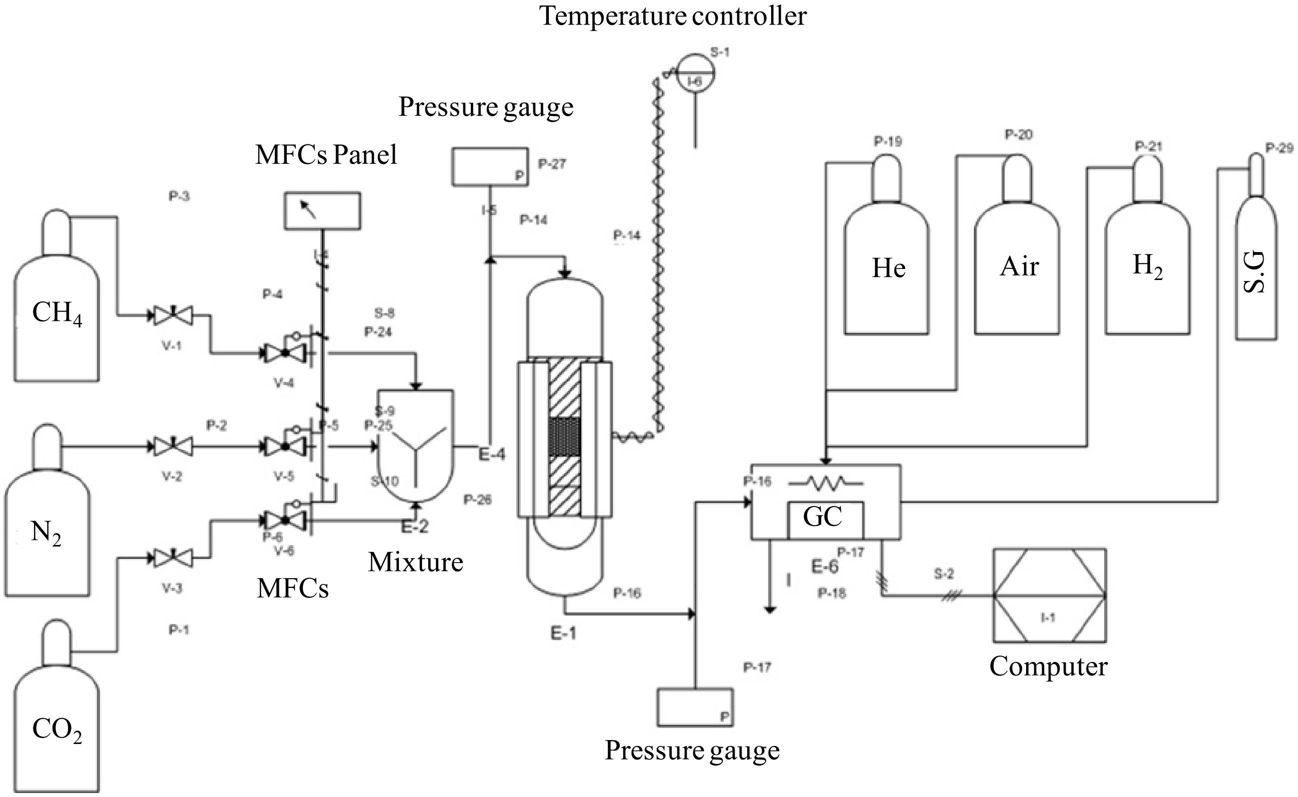

Fig. S1. Schematic diagram of the experimental set-up.

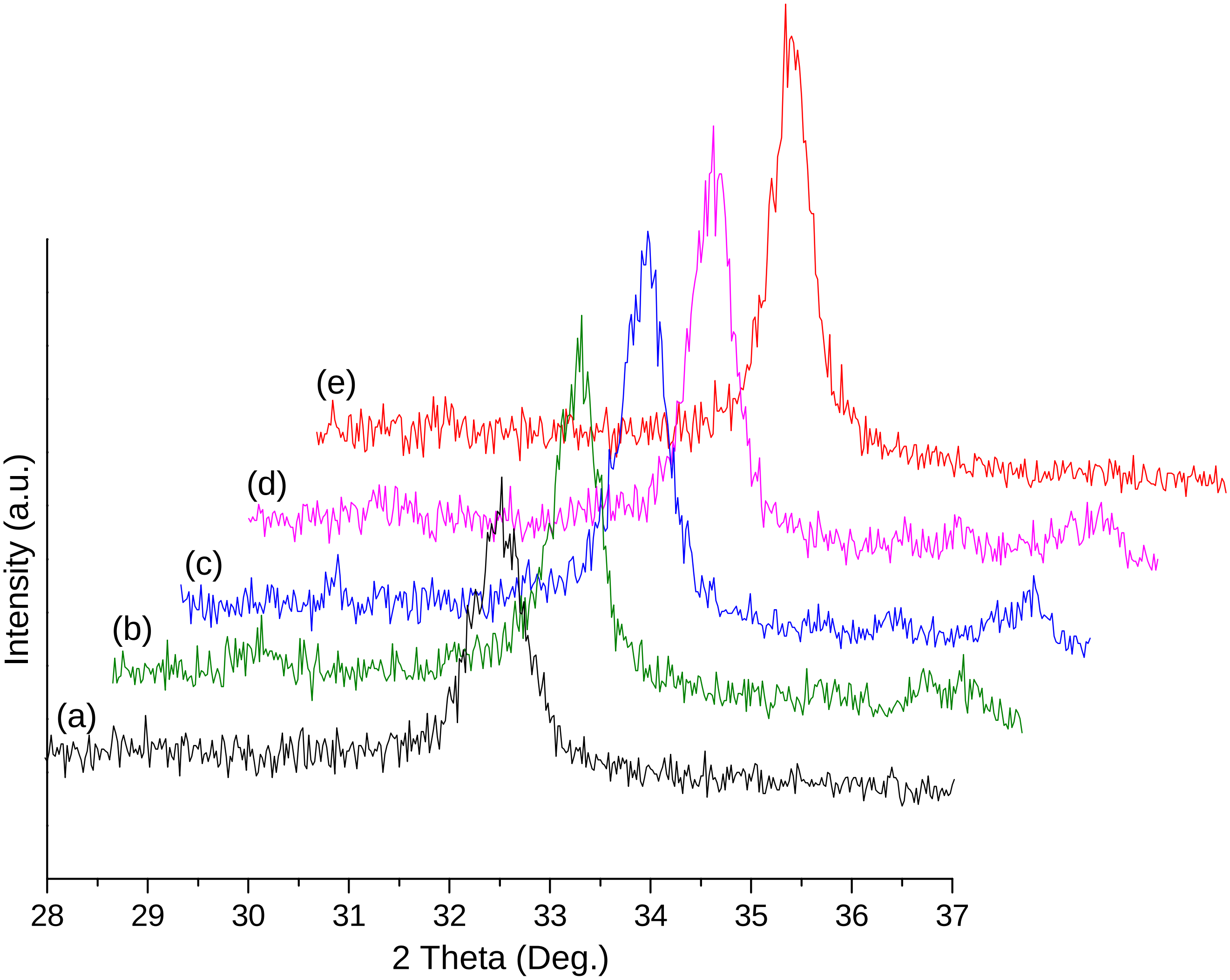

Fig. S2. Evolution of the XRD highest peak of (a) Bulk $La_{0.6}Sr_{0.4}MnO_3$, (b) 3DOM $La_{0.6}Sr_{0.4}MnO_3$, (c) 1.58 wt% Ag/3DOM $La_{0.6}Sr_{0.4}MnO_3$, (d) 3.63 wt% Ag/3DOM $La_{0.6}Sr_{0.4}MnO_3$, and (e) 5.71 wt% Ag/3DOM $La_{0.6}Sr_{0.4}MnO_3$.

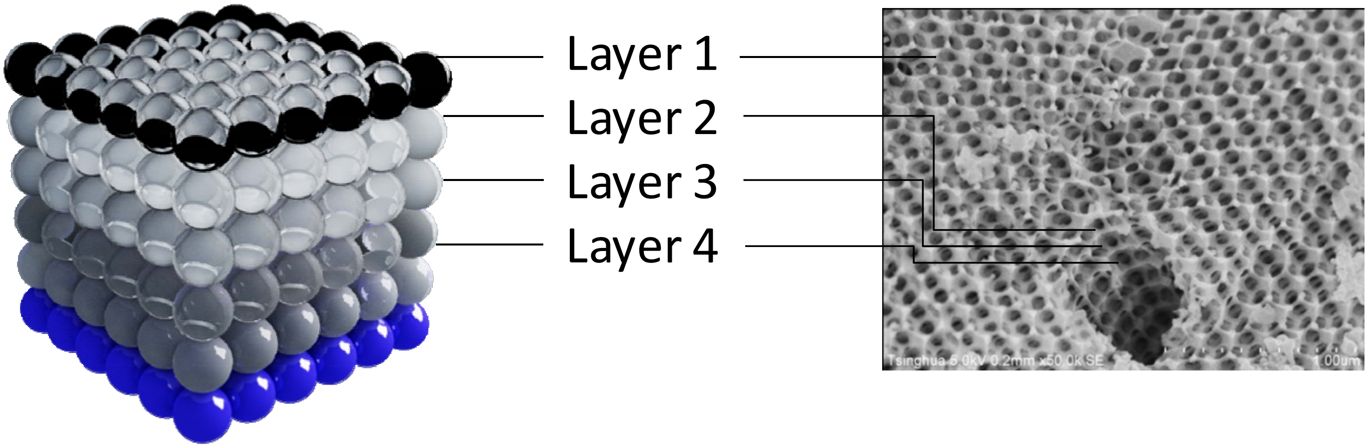

Fig. S3. Four discrete layers with interconnected open windows within each layer.

The introduction of an excess amount of $Ag(NO_3)_2$ had no significant effects on the quality of 3DOM structure (Fig. 1a–c). Meanwhile, the amount of DMOTEG (3.00mL) in the presence of PEG400 (5.00 mL) added to the precursor solution during the preparation process exerted an impact on the crystallite size, and led to the generation of a high-quality 3DOMarchitecture with interconnected macroporous walls of yAg/3DOM $La_{0.6}Sr_{0.4}MnO_3$ (Fig. 1c and Fig. S1).

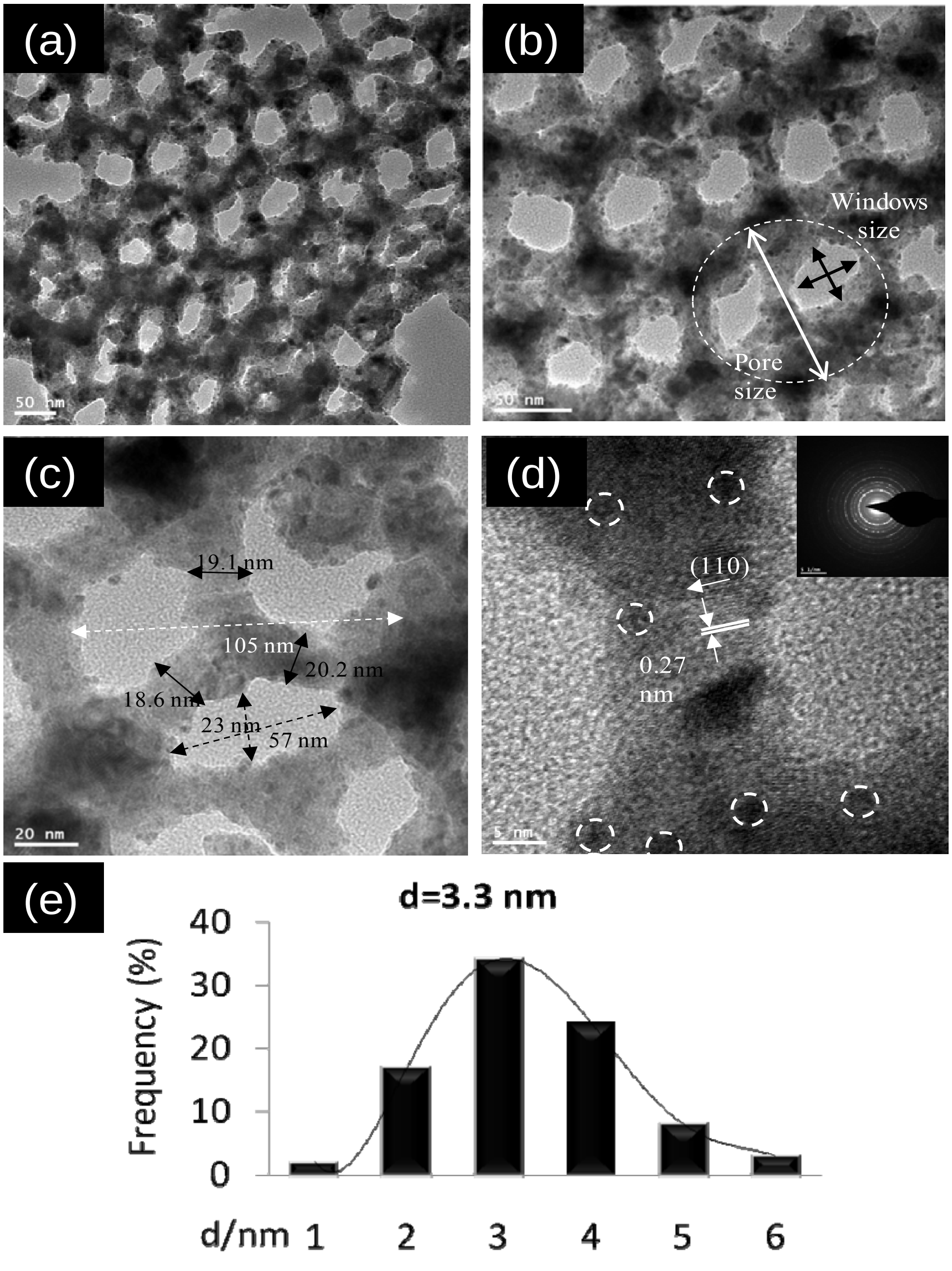

Fig. S4 TEM images (a, b) and HRTEM images (c, d) and size distribution of Ag NPs (e) of 1.58 wt% Ag/3DOM $La_{0.6}Sr_{0.4}MnO_3$.

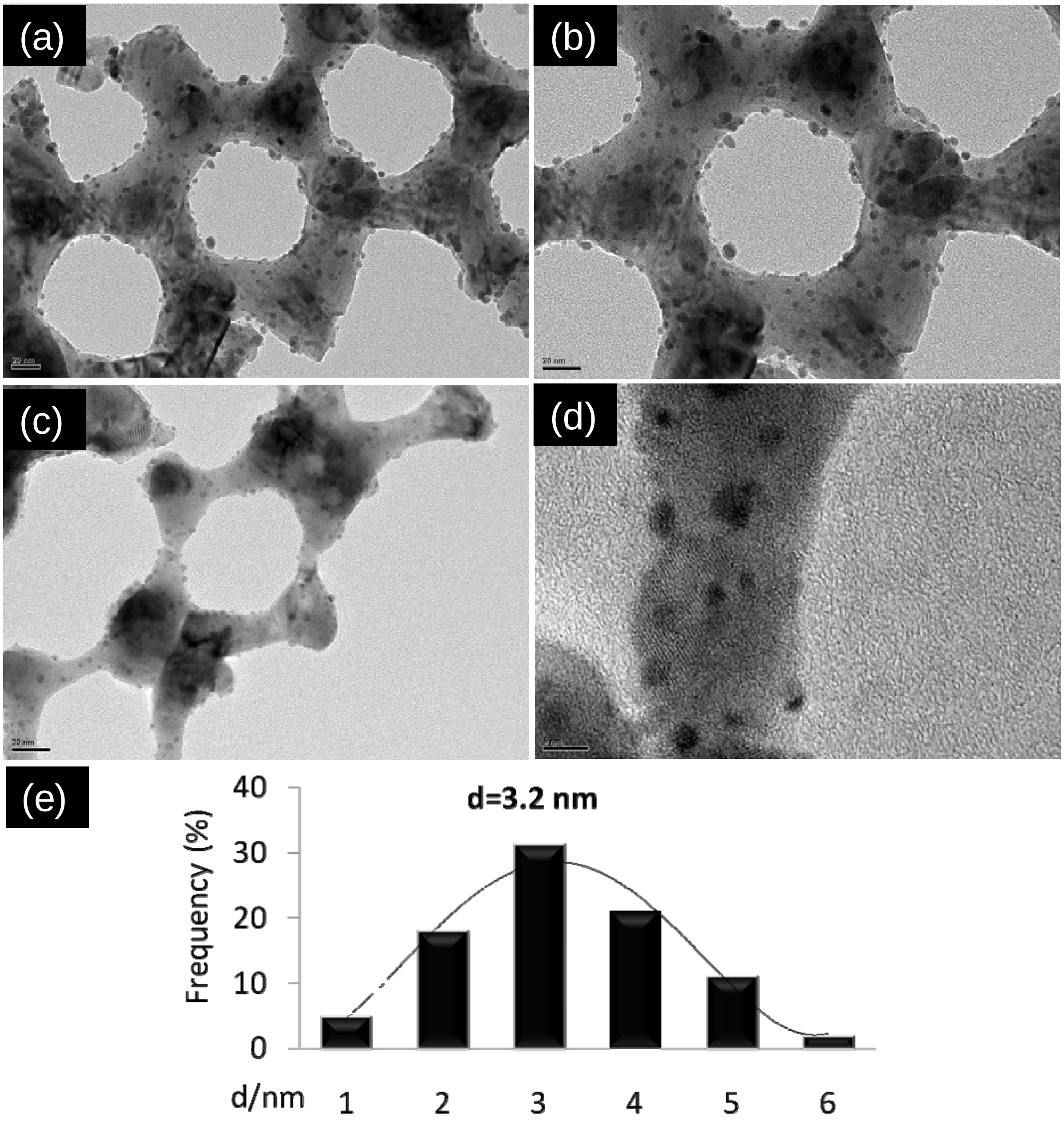

Fig. S5 (a-c) TEM and (d) HRTEM images and size distribution (e) of Ag NPs by statistic analysis of more than 200 Ag particles in HRTEM images of 3.63 wt% Ag/3DOM $La_{0.6}Sr_{0.4}MnO_3$.

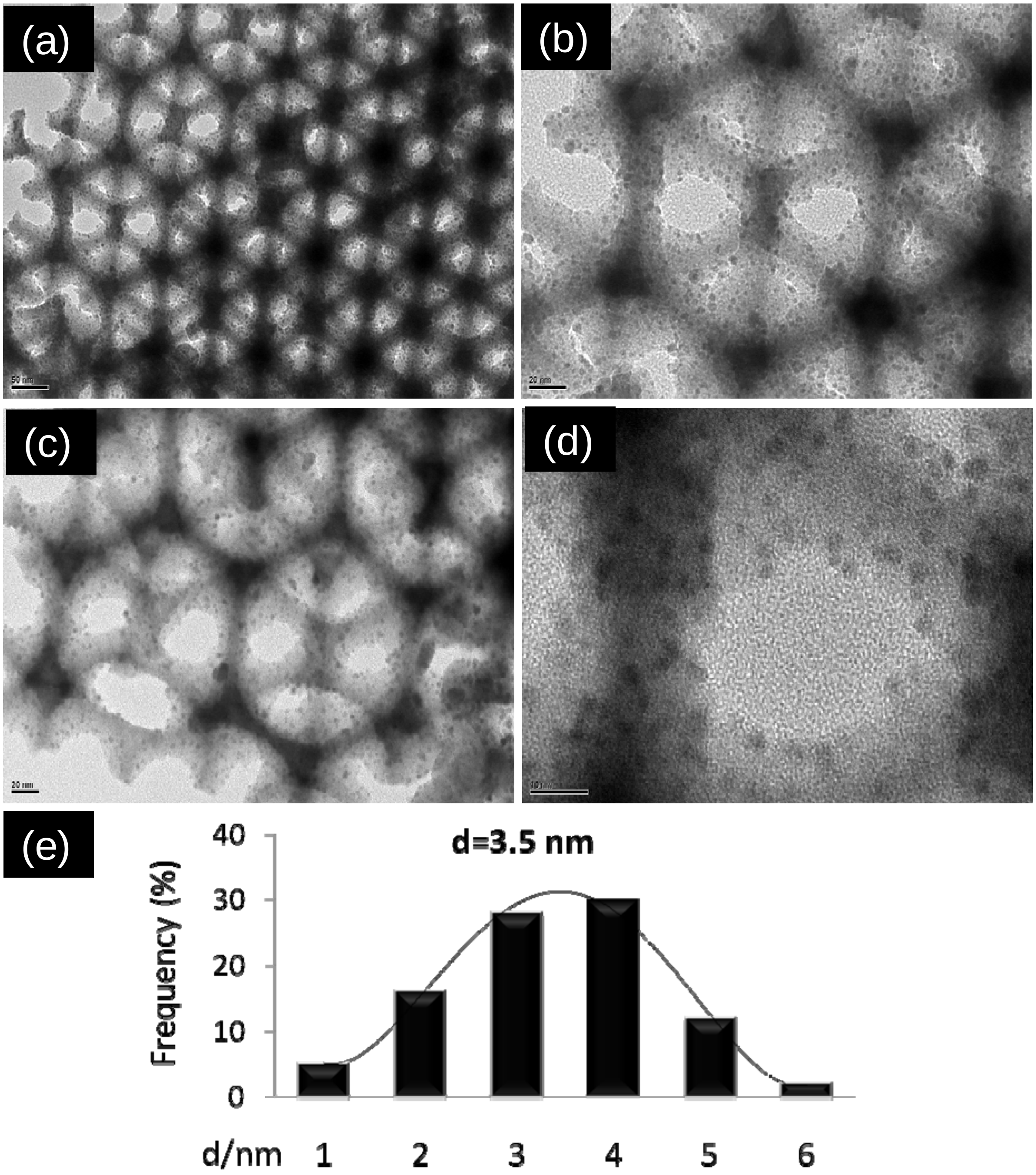

Fig. S6 TEM (a-c) and HRTEM (d) images and size distribution (e) of Ag NPs by statistic analysis of more than 200 Ag particles in HRTEM images of 5.71 wt% Ag/3DOM $La_{0.6}Sr_{0.4}MnO_3$.

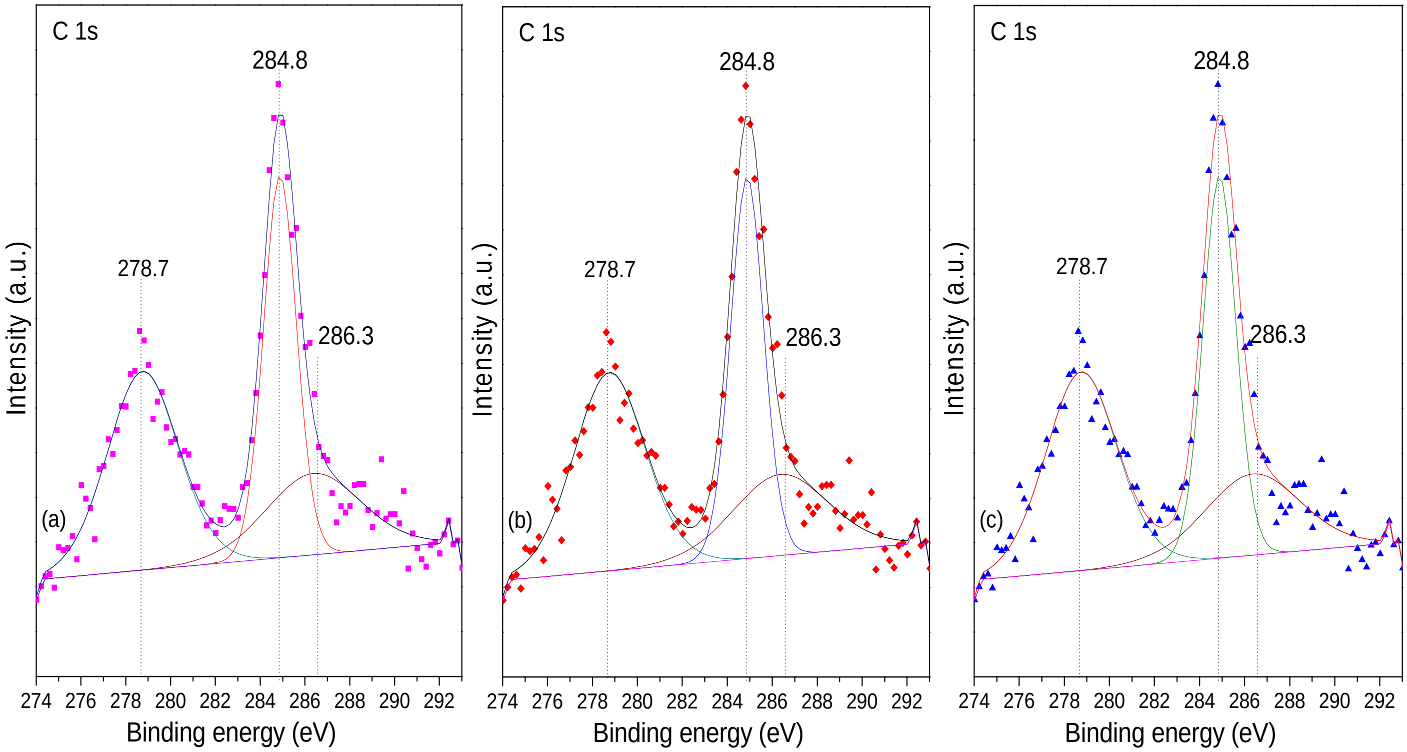

Fig. S7. C 1s XPS spectra of (a) 1.58 wt% Ag/3DOM $La_{0.6}Sr_{0.4}MnO_3$, (b) 3.63 wt% Ag/3DOM $La_{0.6}Sr_{0.4}MnO_3$, and (c) 5.71 wt% Ag/3DOM $La_{0.6}Sr_{0.4}MnO_3$.

C 1s XPS results:

Fig. S7a-c show the C 1s XPS spectra of the three samples. One can clearly observe that there was a similar symmetrical C 1s XPS signals at ca. 278.7 and 284.8 eV for each sample, which generally came from the contaminated carbon. However, another rather weak C 1s signal at BE = ca. 286.3 eV appeared in each of the three samples (1.58 wt% Ag/3DOM $La_{0.6}Sr_{0.4}MnO_3$, 3.63 wt% Ag/3DOM $La_{0.6}Sr_{0.4}MnO_3$, and 5.71 wt% Ag/3DOM

$La_{0.6}Sr_{0.4}MnO_3$) which was due to the surface carbonate species [1, 2]. Therefore, no significant amounts of carbonate species were formed on the surface of the three samples. Although each of the catalyst samples was pretreated in an O_2 flow of 20 mL/min at 450 ^oC for 1 h before XPS measurements, which could minimize the amounts of OH^- and carbonate species retained on the sample surfaces, the presence of carbonate species could not be completely precluded. After carefully examining the C 1s XPS spectra (Fig. S7) of these samples, we decompose each of them to three components at BE = 284.8 and 286.3 eV (due to surface contamination carbon) and 278.7 eV (due to surface carbonate species) [3].

References:

[1] H. Falcón, J. A. Barbero, J. A. Alonso, M. J. Martínez-Lope, J. L. G. Fierro, Chem. Mater. 14 (2002) 2325−2333.

[2] J.L.G. Fierro, Catal. Today 8 (1990) 153−174.

[3] Y.N. Lee, R.M. Lago, J.L.G. Fierro, V. Cortés, F. Sapiña, E. Martínez, Appl. Catal. A 207 (2001) 17–24.

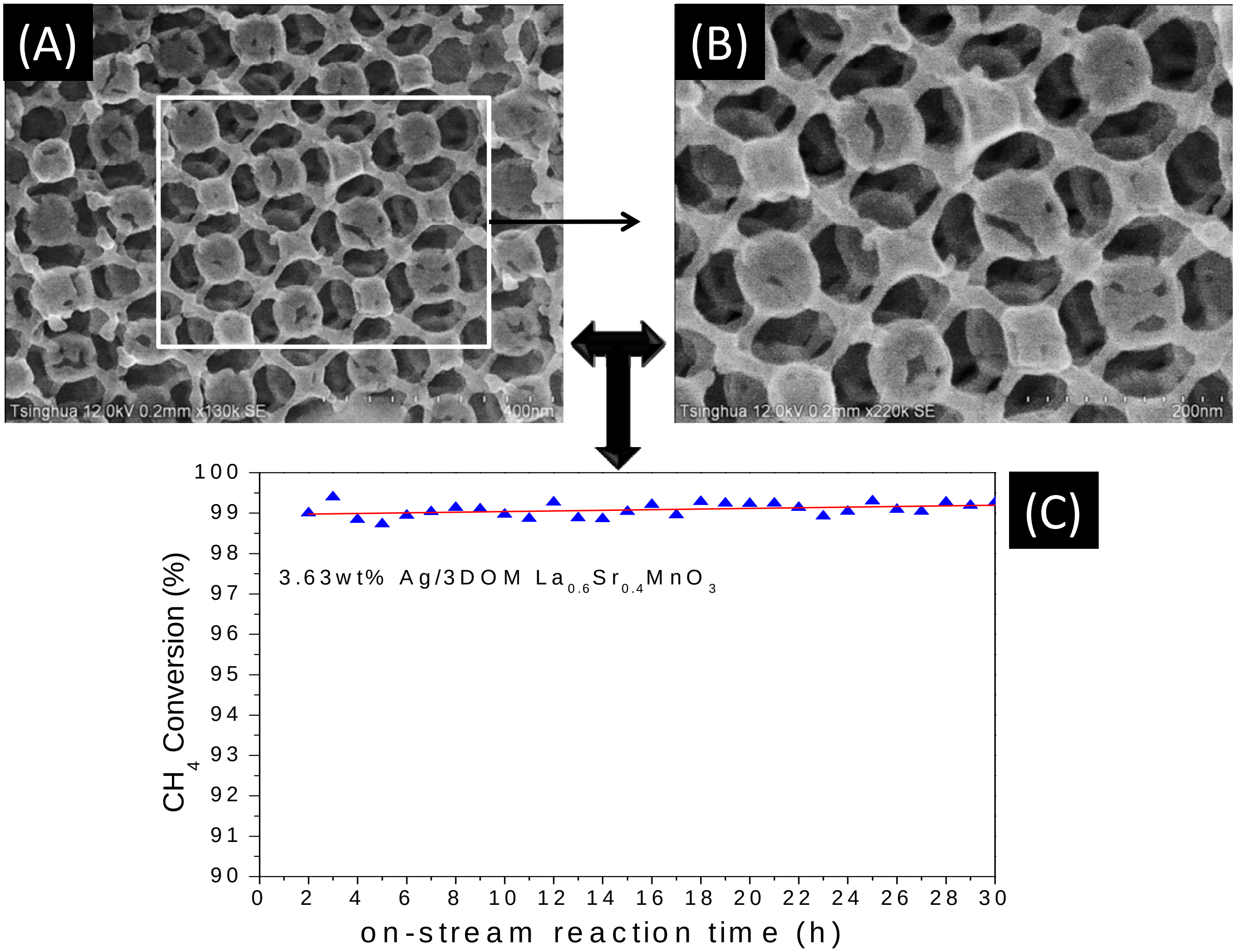

Fig. S8. (A, B) SEM image of 3.63 wt% Ag/3DOM $La_{0.6}Sr_{0.4}MnO_3$ after 30 h of on-stream reaction under the conditions of 2% CH_4 + 20% O_2 + 78% N_2 (balance) and GHSV = 30,000 mL/(g h).

The characterization results from transmission electron microscope (SEM/HRSEM) showed that the prepared catalysts indeed formed the three dimensionally ordered macroporous structures. Fig. S8 shows the SEM and HRSEM images of the 3.63 wt% Ag/3DOM $La_{0.6}Sr_{0.4}MnO_3$ catalyst after catalytic reaction. From the image, it can be seen that the macrostructure of the used catalyst was not remarkably changed after the combustion of CH_4.

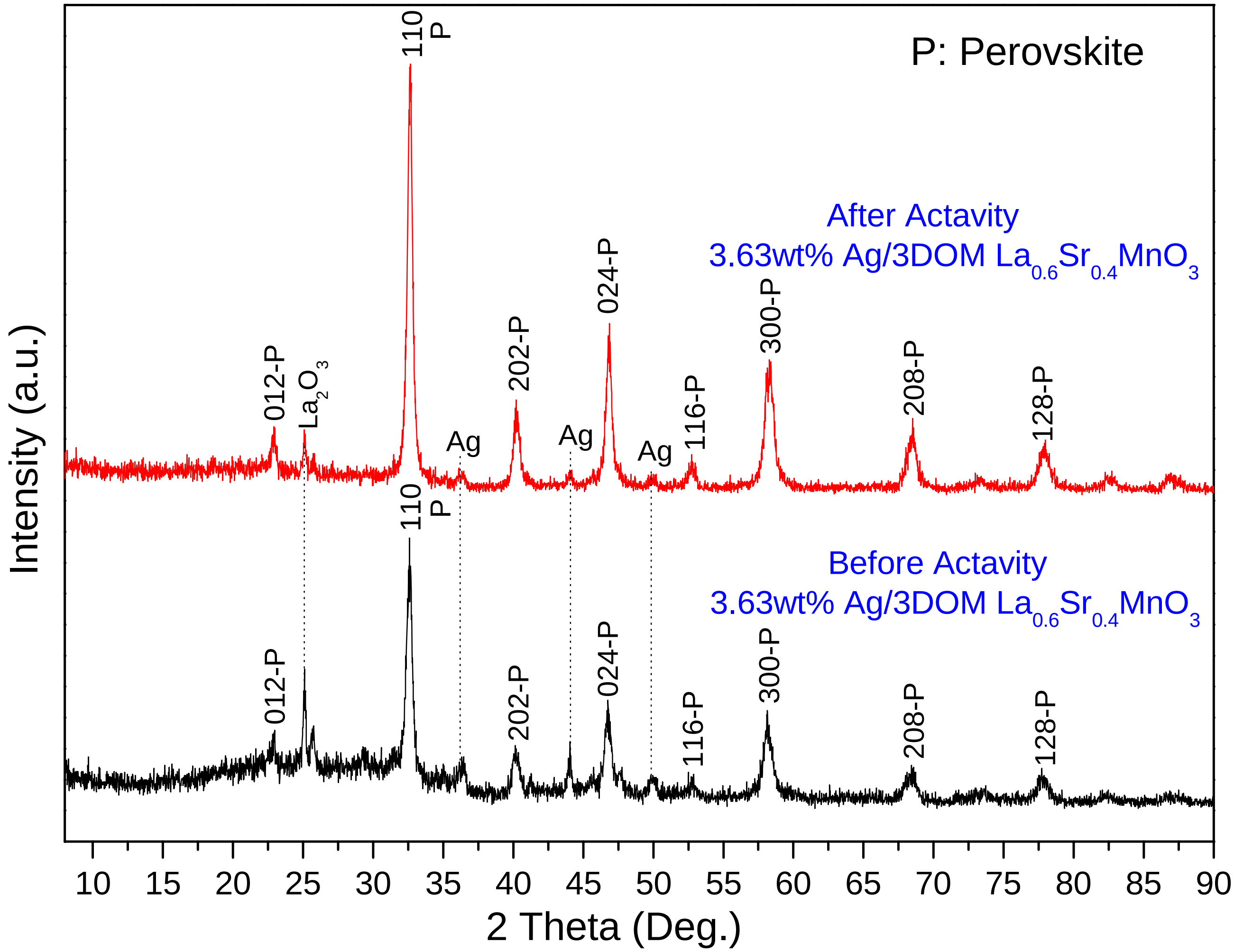

Fig. S9. XRD pattern of the 3.63 wt% Ag/3DOM $La_{0.6}Sr_{0.4}MnO_3$ sample after 20 h of on-stream reaction at GHSV = 30,000 mL/(g h).

It can be seen from Fig. S9 that after 20 h of on-stream reaction, the used 3.63 wt% Ag/3DOM $La_{0.6}Sr_{0.4}MnO_3$ catalyst showed approximately the same XRD pattern as that of the fresh one.

Turnover Frequencies (TOFs)

The TOF_{Ag} and TOF_{Mn} of the samples were calculated under the conditions of CH_4/O_2 molar ratio = 1/10, GHSV = 30,000 mL/(g h), and temperature = 300, and 400 °C, as summarized in Table 1. It is observed that the nonporous bulk-$La_{0.6}Sr_{0.4}MnO_3$ sample at the same temperature, the TOF_{Mn} values of the porous 3DOM $La_{0.6}Sr_{0.4}MnO_3$ and *y*Ag/3DOM $La_{0.6}Sr_{0.4}MnO_3$ samples were much higher. For instance, the TOF_{Mn} value (5.56×10^{-7}) of 3.63 wt% Ag/3DOM $La_{0.6}Sr_{0.4}MnO_3$ was approximately 1.5 times as much as that (4.17×10^{-7}) of 3DOM-$La_{0.6}Sr_{0.4}MnO_3$ for methane combustion at 300 °C. With the rise in Ag NPs loading from 1.58 to 3.63 wt% during the catalyst preparation process, the obtained 1.58 wt% Ag/3DOM $La_{0.6}Sr_{0.4}MnO_3$ and 3.63 wt% Ag/3DOM $La_{0.6}Sr_{0.4}MnO_3$ samples exhibited the TOF_{Mn} values of 5.07×10^{-7} and 7.14×10^{-7} (mol/mol_{Mn} s) at 300 °C, and 5.56×10^{-7} and 9.03×10^{-7} (mol/mol_{Mn} s) at 350 °C, respectively; but they decreased to 5.05×10^{-7} (mol/mol_{Mn} s) at 300 °C and 8.11×10^{-7} (mol/mol_{Mn} s) at 400 °C with a further rise in Ag NPs loading from 3.63 to 5.71 wt%. In the meantime, from Table 1, one can also observe that the TOF_{Ag} (mol/mol_{Ag} s) values (1.86×10^{-5} at 300 °C and 11.8×10^{-5} at 400 °C) of the 3.63 wt% Ag/3DOM $La_{0.6}Sr_{0.4}MnO_3$ sample was much higher than that (1.23×10^{-5} at 300 °C and 7.28×10^{-5} at 400 °C) of the 1.58%wt. Ag/3DOM $La_{0.6}Sr_{0.4}MnO_3$ sample. This result indicates that there was a strong interaction (SMSIs) between the metal (Ag NPs) and the support ($La_{0.6}Sr_{0.4}MnO_3$), which gave rise to an enhanced catalytic performance of *y*Ag/3DOM $La_{0.6}Sr_{0.4}MnO_3$ for methane combustion. The reaction rate (58.7–61.8 μmol/(g s)) for methane oxidation at 550 °C over *y*Ag/3DOM $La_{0.6}Sr_{0.4}MnO_3$ was higher than that (14.2 μmol/(g s)) over 3.6 wt% Au/$LaCoO_3$ [1], but inferior to that (74.3 μmol/(g s)) over 8 wt% Au/MnO_2 [2]. It is worth pointing out that under similar reaction conditions, the catalytic activity ($T_{50\%}$ = 454 °C and $T_{90\%}$ = 524 °C) over our the best-performing 3.63 wt% Ag/3DOM $La_{0.6}Sr_{0.4}MnO_3$ catalyst was much better than those ($T_{50\%}$ = 654 °C and $T_{90\%}$ = 800 °C) over $La_{0.9}Cu_{0.1}MnO_3$ [3], ($T_{50\%}$ = 710 °C and$T_{90\%}$ = 770 °C) over 20 wt% $LaMnO_3$/MgO [4] , ($T_{50\%}$ = 620 °C and $T_{90\%}$ = 710 °C) over $La_{0.5}Sr_{0.5}MnO_3$ [5], ($T_{50\%}$ = 662 °C and $T_{90\%}$ = 739 °C) over La_2CuO_4 nanorods [6], but inferior to those ($T_{50\%}$ = 365 °C and $T_{90\%}$ = 425 °C) over 1 wt% Pd/ZrO_2 [7].

References:

[1] M.L. Jia, Menggentuya, Z. Bao, Y.N. Shen Catalysis Letters, 134 (2010) 87–92.

[2] S. Scirè, L. F. Liotta, Applied Catalysis B: Environmental 125 (2012) 222-246.

[3] G. Bulgan, F. Teng, S. H. Liang, W. Q. Yao, Y. F. Zhu, Wuli Huaxue Xuebao/ Acta Physico - Chimica Sinica 23 (2007) 1387-1392.

[4] E. E. Svensson, S. Nassos, M. Boutonnet, S. G. Järås, Catalysis Today 117 (2006) 484-490.

[5] S. Ponce, M. A. Peña, J. L. G. Fierro, Applied Catalysis B: Environmental 24 (2000) 193-205.

[6] L. Zhang, Y. Zhang, H. Dai, J. Deng, L. Wei, H. He, Catalysis Today 153 (2010) 143-149.

[7] P. Araya, S. Guerrero, J. Robertson, F. J. Gracia, Applied Catalysis A: General 283 (2005) 225-233.